Biochimica et Biophysica Acta 1798 (2010) 94–104

Contents lists available at ScienceDirect

Biochimica et Biophysica Acta

journal homepage: www.elsevier.com/locate/bbamem

Correlating structure, dynamics, and function in transmembrane segment VII of the Na^+/H^+ exchanger isoform 1

Tyler Reddy [a], Xiuju Li [c], Larry Fliegel [c], Brian D. Sykes [c], Jan K. Rainey [a,b,*]

[a] Department of Biochemistry and Molecular Biology, Dalhousie University, Halifax, NS, Canada B3H 1X5
[b] Department of Chemistry, Dalhousie University, Halifax, NS, Canada B3H 1X5
[c] Department of Biochemistry, University of Alberta, Edmonton, AB, Canada T6G 2H7

ARTICLE INFO

Article history:
Received 15 April 2009
Received in revised form 17 June 2009
Accepted 29 June 2009
Available online 23 July 2009

Keywords:
NMR
^{15}N relaxation
Model-Free analysis
Reduced spectral density mapping
DPC
Peptide

ABSTRACT

We place ^{15}N nuclear magnetic resonance relaxation analysis and functional mutagenesis studies in the context of our previous structural and mutagenesis work to correlate structure, dynamics and function for the seventh transmembrane segment of the human Na^+/H^+ exchanger isoform 1. Although G261–S263 was previously identified as an interruption point in the helical structure of this isolated transmembrane peptide in dodecylphosphocholine micelles, and rapid conformational exchange was implicated in the NOE measurements, the six ^{15}N labelled residues examined in this study all have similar dynamics on the ps–ns time scale. A mathematical model incorporating chemical exchange is the best fit for residues G261, L264, and A268. This implies that a segment of residues from G261 to A268 samples different conformations on the μs–ms time scale. Chemical exchange on an intermediate time scale is consistent with an alternating-access cycle where E262 is bent away from the cytosol during proton translocation by the exchanger. The functional importance of chemical exchange at G261–A268 is corroborated by the abrogated activity of the full-length exchanger with the bulky and restricting Ile substitutions F260I, G261I, E262I, S263I, and A268I.

1. Introduction

The α-helical class of integral membrane proteins (*i.e.*, those with primarily α-helical membrane-spanning domains) frequently contain transmembrane (TM) segments with disruptions in canonical helical secondary structure [1,2]. As an example, disruptions in TM helices have been observed for six of the seven TM segments in the rhodopsin crystal structure [3]. These types of disruption have been hypothesized to allow increased structural diversity in spite of the constraints of an α-helical TM domain geometry [2]. Beyond simply expanding the structural toolkit for building of TM domains, these breaks in H-bonded secondary structure have been hypothesized to be critical in function by allowing essential conformational changes in the TM domain of the protein. In the prokaryotic Na^+/H^+ antiporter (NhaA), for example, TM segments IV and XI contain extended disruptions in helicity near the centre of the TM domains [4]. These extended portions of the TM segments are in close proximity to the ion binding site of NhaA in the crystal structure of the low-pH inactivated form. The apparently flexible character of these extended portions of TM IV and XI is proposed to allow switching between the active and inactive conformations. Similar mechanisms have been advanced based upon crystal structures of the sarcoplasmic/endoplasmic reticulum Ca^{2+}/ATPase (SERCA1a; [5]) and a prokaryotic homologue of Na^+/Cl^- dependent neurotransmitter transporters ($LeuT_{AA}$; [6]). Furthermore, both G protein-sensitive inwardly rectifying potassium (GIRK) channels and the potassium channel KcsA depend on helical bending for ion translocation [7]. In fact, a proline substitution in TM II of GIRK, a situation reasonably likely [8] to induce α-helical disruption [2], results in a constitutively active channel [9]. Our solution-state NMR studies of isolated TM segments of the mammalian Na^+/H^+ exchanger isoform 1 (NHE1), an integral α-helical membrane protein with 12 TM domains [10,11], have demonstrated varying degrees of helical disruption in each of four functionally critical TM domains studied to date [12–15]. Notably, the disruptions in helicity in NHE1 TM segments IV and XI have strong similarity to the corresponding segments in NhaA [4], a homolog to NHE1. These structure–function based studies are extended and correlated herein to a quantitative NMR-based determination of dynamics for TM VII of NHE1.

Solution-state NMR has been used extensively to analyze water-soluble peptide and protein dynamics (reviewed in [16,17]). However, insoluble membrane proteins or TM segments of membrane proteins present a challenge for solution-state dynamics analysis. A particularly inventive approach was applied to the potassium channel KcsA. Selective substitution of polar and charged amino acids allowed this

Abbreviations: AIC, Akaike's information criteria; CSA, chemical shift anisotropy; DPC($-d_{38}$), (deuterated) dodecylphosphocholine; NhaA, prokaryotic Na^+/H^+ antiporter; NHE1, Na^+/H^+ exchanger isoform 1; NMR, nuclear magnetic resonance; NOE, nuclear Overhauser effect; TM, transmembrane

* Corresponding author. Department of Biochemistry and Molecular Biology, 5850 College Street, Room 10N, Sir Charles Tupper Medical Building, Dalhousie University, Halifax, NS, Canada B3H 1X5. Tel.: +1 902 494 4632; fax: +1 902 494 1355.
E-mail address: jan.rainey@dal.ca (J.K. Rainey).

0005-2736/$ – see front matter © 2009 Elsevier B.V. All rights reserved.
doi:10.1016/j.bbamem.2009.06.025

membrane protein to be made water-soluble while retaining much of its native structure. This made a detailed analysis of dynamics possible [18]. However, this strategy requires extensive protein engineering combined with some degree of serendipity, potentially needing the production of many water-soluble variants of the native protein before achieving a good mimic [19]. Solid-state NMR methods allow study of membrane proteins in more native-like environments, removing the issue of finding a suitable membrane-mimetic solution environment or of engineering the protein to render it water-soluble. The dynamics of the membrane protein phospholamban were studied in a lipid bilayer using T_2-selective through-bond correlation spectroscopy [20]. This solid-state NMR technique also allowed identification of the structured β-sheet core of fibrillar α-synuclein relative to its highly mobile C-terminus [21]. Application of solid-state NMR techniques to the study of cytochromes P450 and b_5 has been reviewed in detail [22], and the specific application of bicelles as a suitable membrane-mimetic for cytochrome b_5 solid-state experiments has recently been described [23]. A more tractable approach is to study the solution-state dynamics of isolated TM segments, either in the case where a protein only has a single TM domain or as a "dissection" from the full-length protein. Although this relies upon use of membrane-mimetic conditions such as micelles, a number of studies have now demonstrated good agreement between polypeptide structures in the micelle and lipid bilayer states [24–27] or between isolated TM segments in membrane-mimetic environments and their counterparts in crystal structures of the full TM domain [28,29] implying good potential for relevance of micelle-derived results to the membrane state accessible by solid-state NMR. The bacteriophage fd coat protein consists of an amphipathic helix connected by a short loop to a buried hydrophobic helix [30]. The bend angle between helices increases by almost 90° in a membrane versus viral coat environment, providing a link between the structure and biological role of the protein. Residues in the fd loop region are more mobile based on a model-free analysis in sodium dodecyl sulfate (SDS) micelles [30]. A fragment representing a single TM segment of the polytopic membrane protein bacteriorhodopsin was solubilized in 1:1 choloroform/methanol and in SDS micelles, and its ^{1}H–^{15}N dynamics studied in detail [31,32]. The authors conclude that there are significant helix coil transitions and μs time scale chemical exchange occurring at the peptide C-terminus.

In this paper, we use ^{15}N NMR relaxation methods to study the dynamics of a ^{15}N-labelled peptide of TM VII of NHE1 and correlate this to structure (Fig. 1) and functional information. NHE1 has a wide range of biological functions and important roles in certain disease conditions. It is a ubiquitously expressed plasma membrane protein that protects cells from intracellular acidification by exchanging an intracellular proton for an extracellular sodium ion [33]. The exchanger also promotes cell growth and differentiation [34], and regulates cell volume in response to osmotic shrinkage [35]. Inhibition of NHE1 protects the myocardium from damage following ischemia and reperfusion and protects against cardiac hypertrophy [36,37]. We

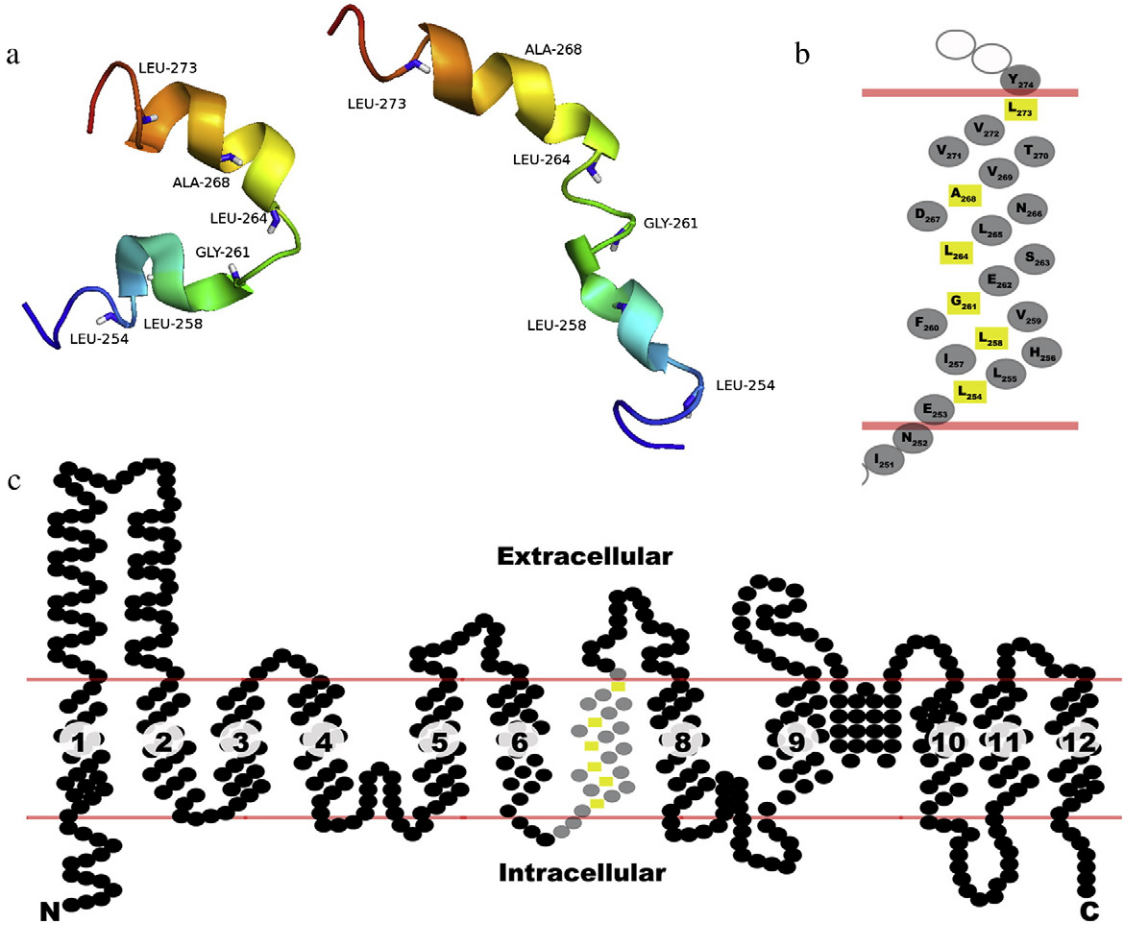

Fig. 1. Structure and topology of NHE1 TM VII. (a) Two structures from the NHE1 TM VII NMR ensemble with very different bend angles about G261–S263 [12]. These conformers are a representative pair that converged under dual-conformer structural calculation protocols [12,63] using all identified NOEs. Specifically, this pair of relative positions of the N- and C-terminal helical segments about the break in helicity at G261–S263 was uniformly obtained in satisfaction of the NOE restraints. The six residues studied by ^{15}N relaxation experiments are labelled and the ^{15}N–H bond vectors are drawn explicitly relative to the backbone Cα cartoon. (b) Crude topological model of TM VII with ^{15}N-labelled residues shown as yellow squares. This is based on the widely accepted topology of the 12 TM segment NHE1 protein obtained by cysteine accessibility mapping and hydropathy analysis [11] shown in (c). Residues comprising TM VII are coloured as in (b). The full-length intracellular C-terminal tail is not shown.

previously studied functional aspects of the full-length NHE1 protein by performing alanine scanning and insertion mutagenesis at the TM VII segment (residues 251–273) [12]. Ala is the fourth most common amino acid in protein TM segments and is the fifth most effective helix-inducer in a hydrophobic environment [8,38]. Ala substitutions at 13 of 22 TM VII residues resulted in severely reduced activity in the full-length NHE1 protein [12]. Beyond perturbing intramolecular interactions or removing key chemical moieties required for ion transport, if flexibility at TM VII is important for NHE1 function (*i.e.*, ion transport) Ala substitutions may interfere by promoting the structural rigidity of an α-helix in addition to replacing important charged or steric residues. The potential importance of flexibility in TM VII is spurred by the ensemble of NMR structures for the peptide in dodecylphosphocholine (DPC) micelles, which show an α-helix interrupted at G261–S263 [12]. E262 is critical to activity in the full-length NHE1 protein and, more specifically, an acidic residue at this position is hypothesized to be important for cation coordination [39]. Since E262D retains much of the NHE1 activity [39], it is possible that the reduced helix forming propensity of acidic residues in comparison to Ala in addition to charge retention is important for conserving both a disruption in helicity and ion coordination [12]. The G261A and E262A mutants of NHE1 were 50% and 48% less active than the wild-type protein, respectively, even after correction for reduced expression and targeting [12]. The G261–S263 region in the TM VII peptide in DPC micelles was found in two predominant conformations, one in which G261–S263 is fairly extended and the N- and C-terminal helical regions are distal to each other and the other in which the helical regions are in close proximity and G261–S263 is allowing the formation of a tight kink ([12]; Fig 1). Observation of a single set of NMR chemical shifts in this region implies relatively rapid interconversion between conformations, and hence a rather dynamic structure for the TM segment despite its reconstitution in DPC micelles. Given the reductions in NHE1 activity following Ala substitution mutagenesis at G261 and E262 that we observed previously [12], a new set of mutations are presented in this paper with the goal of testing the effect of further restriction of motion in the TM VII segment. For this purpose, mutation to Ile was chosen since Ile is the most common amino acid found in protein transmembrane (TM) segments and, of the 20 common amino acids, has the highest propensity for α-helix formation in a hydrophobic environment [8,38]. Herein, our structural observations and Ala- and Ile-scanning mutagenesis results are placed into the unique context of ^{15}N–^{1}H NMR spectroscopy based dynamics measurements.

2. Materials and methods

2.1. Materials

Deuterium oxide (99.9% D), deuterium oxide (99.9% D) with 1% sodium 2,2-dimethyl-2-silapentane-5-sulphonate, and dodecylphosphocholine-d_{38} (DPC-d_{38}; 99.1% D) were purchased from CDN Isotopes (Pointe-Claire, QC, Canada). A 535-PP NMR tube (Wilmad Glass Co., Buena, NJ, USA) was used for all NMR relaxation experiments. Lipofectamine™ 2000 reagent was purchased from Invitrogen and PWO DNA polymerase was from Roche Applied Science.

2.2. Peptide synthesis and purification

The TM VII peptide (HINE***L***LHI***L***VF***G***ES***L***LND***A***VTVV***L***YKK; free N-terminus, amide-capped C-terminus; the bold/italicized residues having backbone ^{15}N labels) was synthesized using solid-phase Boc chemistry [40] and purified as previously described [12]. Peptide identity was confirmed by matrix-assisted laser desorption ionization mass spectrometry and by amino acid analysis (Institute for Biomolecular Design, Edmonton, AB, Canada).

Table 1
NMR parameters for ^{15}N relaxation experiments at 500, 600, and 800 MHz.

Experiment	Spectrometer (MHz)	nt	at (s)	d1 (s)	Relaxation delay [s]; interval (s)
R_1	500	1024	0.073	5.0	[0.01, 0.05, 0.1, 0.2, 0.3, 0.5, 0.8]
	600	256	0.061	5.0	[0.01, 0.05, 0.1, 0.2, 0.3, 0.5, 0.8]
	800	256	0.085	10.0	[0.01, 0.05, 0.1, 0.2, 0.3, 0.5, 0.8]
R_2	500	1024	0.073	5.0	[0.01–0.11]; (0.02)
	600	256	0.061	5.0	[0.01–0.11]; (0.02)
	800	256	0.085	10.0	[0.01–0.11]; (0.02)
{^{1}H}–^{15}N NOE	500	16384	0.073	3.0	–
	600	8192	0.061	3.0	–
	800	8192	0.085	3.0	–

2.3. NMR spectroscopy

The NMR sample was prepared by dissolving ~770 μM TM VII peptide in 90% H_2O, 10% D_2O solution containing ~75 mM DPC-d_{38}. Chemical shifts were referenced to 2,2-dimethyl-2-silapentane-5-sulfonic acid at 1.0 mM. Solution pH was adjusted to 4.8 (deuterium isotope effects not taken into account), and all experiments were carried out at 30 °C for consistency with structural studies [12]. ^{1}H observed, ^{15}N NMR relaxation experiments were performed on 500, 600, and 800 MHz (800 equipped with cryogenic probe) Varian Inc. (Palo Alto, CA, USA) INOVA spectrometers, with parameters listed in Table 1. The BioPack (Varian Inc.) gNhsqc pulse sequence [41] was used for measurement of ^{15}N relaxation of labelled TM VII residues. The ^{15}N relaxation rates were measured from 1D {^{1}H–^{15}N}-HSQC spectra. All spectra were processed and analyzed with VnmrJ 2.1B (Varian Inc.).

2.4. ^{15}N relaxation parameters

^{15}N relaxation time constants (T_1, T_2) and their standard errors from the covariance matrix were calculated using a nonlinear least-squares fit to a two parameter monoexponential decay using xcrvfit version 4.0.12.[1] Errors for the first order rate constants (R_1, R_2) were propagated [42] from the time constant errors using:

$$\delta R_i = \frac{|R_i|}{|T_i|}\delta T_i \tag{1}$$

where R_i and T_i represent a pair of rate and time constants, respectively.

Steady-state {^{1}H}–^{15}N NOE values were calculated using the software relax version 1.3.2 [43,44] as the peak height (I) ratios in proton saturated versus reference spectra:

$$\mathrm{NOE} = \frac{I_{\mathrm{sat}}}{I_{\mathrm{ref}}}. \tag{2}$$

Standard deviation ($\boldsymbol{\sigma}$) was propagated from the root-mean-square baseline noise as previously reported [45]:

$$\sigma_{\mathrm{NOE}} = \mathrm{NOE}\left[\left(\frac{\sigma_{I_{\mathrm{sat}}}}{I_{\mathrm{sat}}}\right)^2 + \left(\frac{\sigma_{I_{\mathrm{ref}}}}{I_{\mathrm{ref}}}\right)^2\right]^{1/2}. \tag{3}$$

2.5. Model-free calculations

The calculated T_1, T_2, and NOE values at three field strengths were used to determine the model-free parameters τ_M (overall rotational

[1] http://www.bionmr.ualberta.ca/bds/software/xcrvfit/.

correlation time), S^2 (generalized order parameter) and τ_e (effective internal correlation time) through spectral density function fitting using the following relaxation expressions [46,47]:

$$1/T_1 = \left(d^2/4\right)[J(\omega_H - \omega_N) + 3J(\omega_N) + 6J(\omega_H + \omega_N)] + c^2 J(\omega_N) \quad (4)$$

$$1/T_2 = \left(d^2/8\right)[4J(0) + J(\omega_H - \omega_N) + 3J(\omega_N) + 6J(\omega_H) + 6J(\omega_H + \omega_N)] + \left(c^2/6\right)[3J(\omega_N) + 4J(0)] \quad (5)$$

$$\mathrm{NOE} = 1 + \left(d^2/4\right)(\gamma_H/\gamma_N)[6J(\omega_H + \omega_N) - J(\omega_H - \omega_N)]T_1 \quad (6)$$

where $d = \left[\mu_0 h \gamma_N \gamma_H / \left(8\pi^2\right)\right]\langle 1/r_{NH}^3\rangle$, $c = \left(\omega_N/\sqrt{3}\right)(\sigma_{II} - \sigma_\perp)$, μ_0 is the permeability of free space, ω_N and ω_H are the respective nuclear Larmor frequencies of ^{15}N and ^{1}H, γ_N and γ_H are the respective gyromagnetic ratios of ^{15}N and ^{1}H, h is Planck's constant, r_{NH} is the length of the amide bond, and σ_{II} and $\sigma_\perp$ are the parallel and perpendicular components of the axially symmetric chemical shift tensor. A value of −160 ppm was used for $(\sigma_{II} - \sigma_\perp)$ [45,48]. The form of the spectral density function used in the Lipari–Szabo formalism is given by [49,50]:

$$J(\omega) = 2/5\left\{S^2\tau_M/\left[1 + \left(\omega^2\tau_M^2\right)\right] + \left(1 + S^2\right)\tau/\left[1 + (\omega\tau)^2\right]\right\} \quad (7)$$

where $1/\tau = 1/\tau_M + 1/\tau_e$.

Fitting of the model-free parameters τ_M, S^2, and τ_e to the relaxation data was performed using a suite of Mathematica (Wolfram Research Inc., Champaign, IL, USA) notebooks previously described [51] but modified by Spyracopoulos to include data collected at multiple field strengths in a single calculation. Briefly, five forms of the spectral density function are considered to account for mixtures of motion on various time scales [51,52]. An optimization procedure is performed to fit the experimental input (T_1, T_2, steady-state NOE) to each of these five mathematical models, labelled 1–5. The appropriate model for each of the residues is selected using the statistical approach of Akaike's information criteria (AIC) [53], and 100 Monte Carlo simulations were performed to estimate parameter errors [54].

2.6. Reduced spectral density mapping

Using the reduced spectral density mapping approach [47,55], measurement at three fields strengths for the steady-state NOE, spin-lattice (T_1) and spin–spin (T_2) relaxation times of ^{15}N allows for sampling of seven spectral density values describing the motion of the system [56]. The spectral density values, under the high frequency approximation that $J(0.921\omega_H)$ and $J(0.955\omega_H)$ are both equivalent to $J(0.870\omega_H)$ [47], are obtained from the following set of equations:

$$\mathrm{NOE} = 1 + \left(d^2/4\right)(\gamma_H/\gamma_N)[5J(0.870\omega_H)]T_1 \quad (8)$$

$$R_1 = \left(d^2/4\right)[3J(\omega_N) + 7J(0.870\omega_H)] + c^2 J(\omega_N) \quad (9)$$

$$R_2 = \left(d^2/8\right)[4J(0) + 3J(\omega_N) + 13J(0.870\omega_H)] + \left(c^2/6\right)[3J(\omega_N) + 4J(0)] \quad (10)$$

Eqs. (8)–(10) allow solving for the three unknown spectral density functions $J(0.870\omega_H)$, $J(\omega_N)$, and $J(0)$. The field-dependent $J(0.870\omega_H)$ and $J(\omega_N)$ alongside the field-independent $J(0)$ give seven spectral density values for a given bond vector at three field strengths. Uncertainties in the values of spectral density functions were calculated by propagating the uncertainties of the independent variables using a sum of squares equation:

$$\delta q = \sqrt{\left(\frac{\partial q}{\partial x}\delta x\right)^2 + \ldots + \left(\frac{\partial q}{\partial z}\delta z\right)^2} \quad (11)$$

where $x \ldots z$ represent any number of independent variables and δ values are parameter uncertainties [42].

2.7. Theoretical calculations

The software Maple 11.02 (Waterloo Maple, Inc., Waterloo, ON, Canada) was used to predict the trend for T_1, T_2 or NOE as a function of magnetic field strength according to Eqs. (4)–(7). Specifically, each of the three model-free parameters used to describe the motion of a ^{15}N–H bond vector (S^2, τ_e, τ_M) was independently varied to study the robustness of the trend of T_1, T_2 or NOE with increasing magnetic field strength. τ_M of the NHE1 TM VII peptide in DPC micelles was estimated using a T_1/T_2 fit strategy in the Mathematica notebooks introduced above, as previously described [45,51].

2.8. Site-directed mutagenesis

Mutations were made to an expression plasmid (pYN4+) containing a hemagglutinin (HA) tagged human NHE1 isoform of the Na^+/H^+ exchanger. The plasmid contained the cDNA for the entire coding region of the Na^+/H^+ exchanger and we have previously shown that the HA tag does not affect the function of the protein [57]. Site-directed mutagenesis was done via amplification with PWO DNA polymerase (Roche Molecular Biochemicals, Mannheim, Germany) using the Stratagene (La Jolla, CA, USA) QuikChange™ site-directed mutagenesis kit. Mutations created a restriction enzyme site for use in screening transformants. The fidelity of DNA amplification was confirmed by DNA sequencing. Sequence details are presented in Table 2.

2.9. Cell culture and transfections

Stable cell lines were made of NHE1 expressing cells of all mutants as described earlier [57]. After transfection of AP-1 cells with LIPOFECTAMINE™ 2000 Reagent (Invitrogen Life Technologies, Carlsbad, CA, USA) selection was done using 800 μg/ml geneticin (G418). AP-1 cells lack an endogenous Na^+/H^+ exchanger [15]. Stable cell lines were regularly re-established from frozen stocks at passage numbers between 5 and 9. For each mutant several independently isolated cells lines were characterized and results are shown of one typical isolate.

2.10. SDS-PAGE and immunoblotting

Western blot analysis was used to confirm NHE1 expression [57] in stable cell lines. Cell lysates were made from the cell lines and equal

Table 2
Oligonucleotides used for site-directed mutagenesis of TM VII.

Mutation	Oligonucleotide sequence	Restriction site
F260I	5′-GAGCTGCTGCACATaCTaGTT**aTa**GGGGAGTCCTTGC-3′	SpeI
G261I	5′-CACATCCTTGTTTTT**atc**GAagCTTGCTCAATGACGCC-3′	HindIII
E262I	5′-CCTTGTTTTTGGG**ata**TCCTTGCTCAATGAC-3′	EcoRV
S263I	5′-CTTGTTTTTGGGGAG**atC**TTGCTCAATGACG-3′	BglII
A268I	5′-CCTTGCTCAATGA**tat**CGTCACTGTGGTCC-3′	EcoRV

Mutated nucleotides are in lowercase letters. Mutated nucleotides of changed amino acid residues are in boldface type, and new restriction sites are underlined. Restriction sites created are indicated.

amounts of up to 100 μg of each sample was resolved on a 10% SDS/polyacrylamide gel. Nitrocellulose transfers were immunostained using an anti-HA monoclonal primary antibody (Boehringer Mannheim, Laval, QC, Canada) which reacted with the tag on the exogenous NHE1 protein. Peroxidase-conjugated goat anti-mouse antibody was the secondary antibody (Bio/Can, Mississauga, ON, Canada). Chemiluminescence blotting (Amersham, Little Chalfont, UK) was used to visualize immunoreactive proteins. NIH Image 1.63 software (National Institutes of Health, Bethesda, MD, USA) was used for densitometric analysis of expression levels and surface processing.

2.11. Cell surface expression

To quantify the level of targeting to the cell surface sulfo-NHS-SS-biotin (Pierce Chemical Company, Rockford, IL, USA) was used to

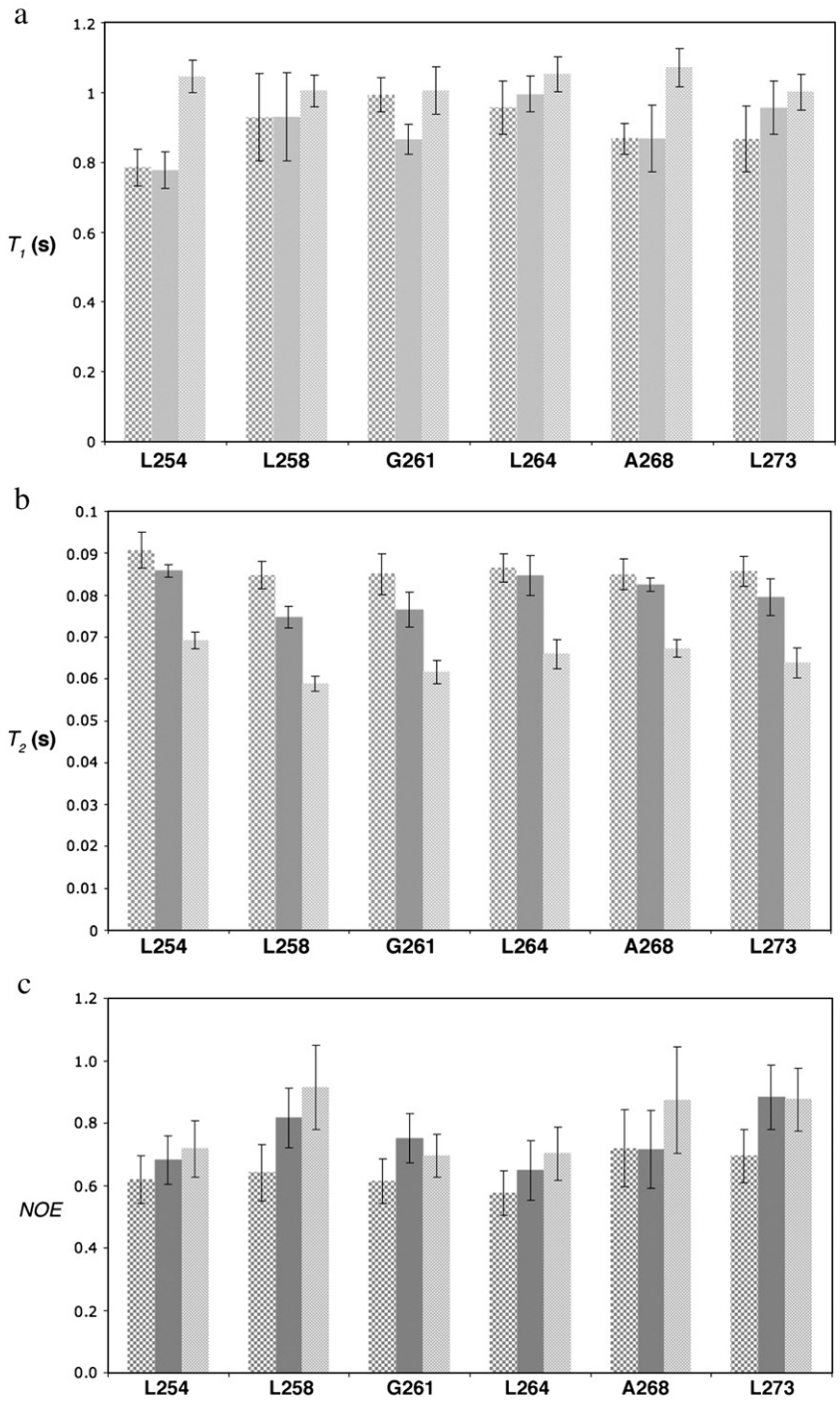

Fig. 2. ^{15}N relaxation parameters compared for the six ^{15}N-labelled TM VII residues at three magnetic field strengths. 500 MHz (checkerboard pattern), 600 MHz (solid gray) and 800 MHz (hatched lines) values for (a) the spin-lattice relaxation time (T_1), (b) the spin–spin relaxation time (T_2), and (c) the steady-state NOE, are plotted as a function of primary sequence with numbering as in the full-length protein. T_1 and T_2 values and their standard errors from the covariance matrix were calculated using the software xcrvfit version 4.0.12 while identical NOE/noNOE peak intensity ratios and errors values were calculated using Microsoft Excel and the software relax version 1.3.2 [43,44], as detailed in Materials and methods.

label cell surface proteins as described earlier [57]. After labelling immobilized streptavidin resin was used to remove plasma membrane labelled Na^+/H^+ exchanger. Equal amounts of total and unbound proteins were separated on SDS-PAGE and Western blotting against the HA tag revealed the amount of NHE1 in different fractions [57]. The amount of NHE1 on the cell surface was calculated by comparing both the 110 kDa and 95 kDa HA-immunoreactive species. It was not possible to efficiently elute proteins bound to immobilized streptavidin resin reproducibly so this fraction was not analyzed.

2.12. Na^+/H^+ exchange activity

Na^+/H^+ exchange activity was measured as described earlier [15]. An acute acid load was induced by ammonium chloride and the initial rate of Na^+-induced recovery of cytosolic pH (pH_i) was measured using 2′,7-bis(2-carboxyethyl)-5(6) carboxyfluorescein-AM (BCECF-AM; Molecular Probes Inc., Eugene, OR, USA). pH measurements were with a PTI (Birmingham, NJ, USA) Deltascan spectrofluorometer. Recovery from acidosis was in the presence of 135 mM NaCl and the initial 20 s of recovery was measured. There was no difference in the buffering capacities of the various stable cell lines and rates of recovery were measured from cells acidified to the same levels. Where indicated, the Na^+/H^+ exchanger activity was corrected for targeting of the protein to the cell surface and for the level of protein expression. Results are the mean ± SE and statistical significance was determined using the Mann–Whitney *U* test.

3. Results

3.1. Relaxation parameters: T_1, T_2, and NOE

A set of ^{15}N NMR relaxation data ($T_1 = 1/R_1$, $T_2 = 1/R_2$, and NOE) was acquired at 500, 600, and 800 MHz for a specifically ^{15}N labelled TM VII peptide in DPC micelles at 30 °C. The T_1 values are similar for all six ^{15}N-labelled TM VII residues, with slightly lower values for L254 at 500 MHz and 600 MHz but not at 800 MHz (Fig. 2a). There is a trend toward increasing T_1 at higher field strength, although the increase is within the bounds of experimental error. In contrast, T_2 values clearly decrease at higher magnetic field strength (Fig. 2b). For each magnetic field strength, the T_2 values are approximately constant over the six residues. The steady-state NOE values are also approximately constant over the six ^{15}N-labelled residues at a given field strength (Fig. 2c). Although NOE values compared between different field strengths overlap within the bounds of experimental error, there is a trend toward increasing NOE at higher field. The complete set of relaxation parameter values and errors are presented in Table 3.

3.2. Reduced spectral density mapping

$J(0.870\omega_H)$, calculated directly from Eq. (8), is plotted for the six ^{15}N-labelled TM VII residues and values are compared between field strengths in Fig. 3a. The general trend is a decrease in $J(0.870\omega_H)$ with increasing field strength, although there is overlap between values within the bounds of experimental error, and in the case of G261 $J(0.870\omega_H)$ is slightly greater at 800 MHz versus 600 MHz. From a sequential standpoint, all six ^{15}N-labelled residues have very similar $J(0.870\omega_H)$ (Fig. 3a). Using the calculated $J(0.870\omega_H)$ and experimental T_1 values, Eq. (9) can be solved for $J(\omega_N)$. $J(\omega_N)$ values calculated from 500 MHz and 600 MHz experiments overlap within the bounds of experimental error, but values calculated from 800 MHz data are clearly smaller (Fig. 3b). In terms of primary sequence, none of the six ^{15}N-labelled residues differs within the bounds of experimental error (Fig. 3b). Finally, experimental T_2 values and calculated $J(\omega_N)$ and $J(0.870\omega_H)$ values can be used to solve Eq. (10) for $J(0)$. There is considerable overlap in $J(0)$ across field strengths within the bounds of experimental error, although there is a trend toward higher values at 800 MHz (Fig. 3c). However, from a sequential standpoint, none of the six residues has a significantly different $J(0)$ at a given field strength (Fig. 3c).

3.3. Model-free analysis

The most common analysis of ^{15}N amide relaxation data for proteins and peptides is the Lipari–Szabo model-free approach where three parameters (S^2, τ_e and τ_M) describe the motion of a ^{15}N-H bond vector based on spectral density functions (*i.e.*, Eq. (7)) [49,50]. The complete model-free results are summarized in Table 4. For L254, L258, and L273, AIC selection favored model five, but each fit had a highly skewed X^2 distribution so the next most likely model was chosen (Table 4). This is also preferable because model five has the most fitting parameters (four) which can increase the strength of fit independent of its true reflection of the empirical relaxation data. The AIC approach selected model four for G261, L264, and A268, which includes a chemical exchange term, R_{ex} — defined as a relaxation contribution from μs–ms time scale motions [47]. This is consistent with a strand of the peptide spanning from G261 to A268 that is subject to chemical exchange. G261 has a slightly lower order parameter ($S^2 = 0.65 \pm 0.02$) than the other five ^{15}N-labelled residues ($S_{average}{}^2 = 0.80 \pm 0.02$). For G261, the slightly reduced order parameter is not consistent with an elevated $J(0)$ (Fig. 3c). Although neither J(0) or S^2 is remarkably different from those of the other five residues, it is noteworthy that chemical exchange (R_{ex}) motions in the μs–ms range can inflate $J(0)$ for affected residues [56,58]:

$$J(0)_{obs} = J(0)_{corr} + \lambda R_{ex} \quad (12)$$

where λ is a positive scaling factor ($\lambda = (3/2)[1/(3d^2 + c^2)]$); *c* and *d* are the chemical shift and dipolar constants defined in the Materials and methods; and, $J(0)_{obs}$ and $J(0)_{corr}$ are the values before and after correction for the contribution from chemical exchange, respectively. Since G261 has the largest R_{ex} value estimated from model-free analysis ($1.9 \pm 0.2\ s^{-1}$) (Table 4), it is certainly possible that chemical exchange can account for the discrepancy of $J(0)_{obs}$ and order parameter for G261. We avoid a more detailed consideration of

Table 3
Longitudinal (R_1) and transverse (R_2) ^{15}N amide relaxation rates and {^1H}-^{15}N NOE.

Residue	R_1 (s^{-1}) 500 MHz	R_1 (s^{-1}) 600 MHz	R_1 (s^{-1}) 800 MHz	R_2 (s^{-1}) 500 MHz	R_2 (s^{-1}) 600 MHz	R_2(s^{-1}) 800 MHz	NOE 500 MHz	NOE 600 MHz	NOE 800 MHz
L254	1.28 ± 0.08	1.29 ± 0.09	0.96 ± 0.04	11.02 ± 0.52	11.65 ± 0.20	14.47 ± 0.41	0.62 ± 0.08	0.68 ± 0.08	0.72 ± 0.09
L258	1.08 ± 0.14	1.07 ± 0.15	1.00 ± 0.04	11.80 ± 0.46	13.38 ± 0.46	16.99 ± 0.53	0.64 ± 0.09	0.82 ± 0.10	0.91 ± 0.14
G261	1.01 ± 0.05	1.15 ± 0.06	0.99 ± 0.07	11.76 ± 0.68	13.06 ± 0.71	16.23 ± 0.72	0.61 ± 0.07	0.75 ± 0.08	0.70 ± 0.07
L264	1.04 ± 0.08	1.00 ± 0.05	0.95 ± 0.04	11.56 ± 0.44	11.81 ± 0.66	15.16 ± 0.79	0.58 ± 0.07	0.65 ± 0.10	0.70 ± 0.09
A268	1.15 ± 0.06	1.15 ± 0.13	0.93 ± 0.05	11.77 ± 0.52	12.13 ± 0.24	14.86 ± 0.47	0.72 ± 0.12	0.72 ± 0.12	0.87 ± 0.17
L273	1.15 ± 0.13	1.05 ± 0.08	1.00 ± 0.05	11.68 ± 0.49	12.58 ± 0.69	15.66 ± 0.88	0.69 ± 0.09	0.88 ± 0.10	0.88 ± 0.10

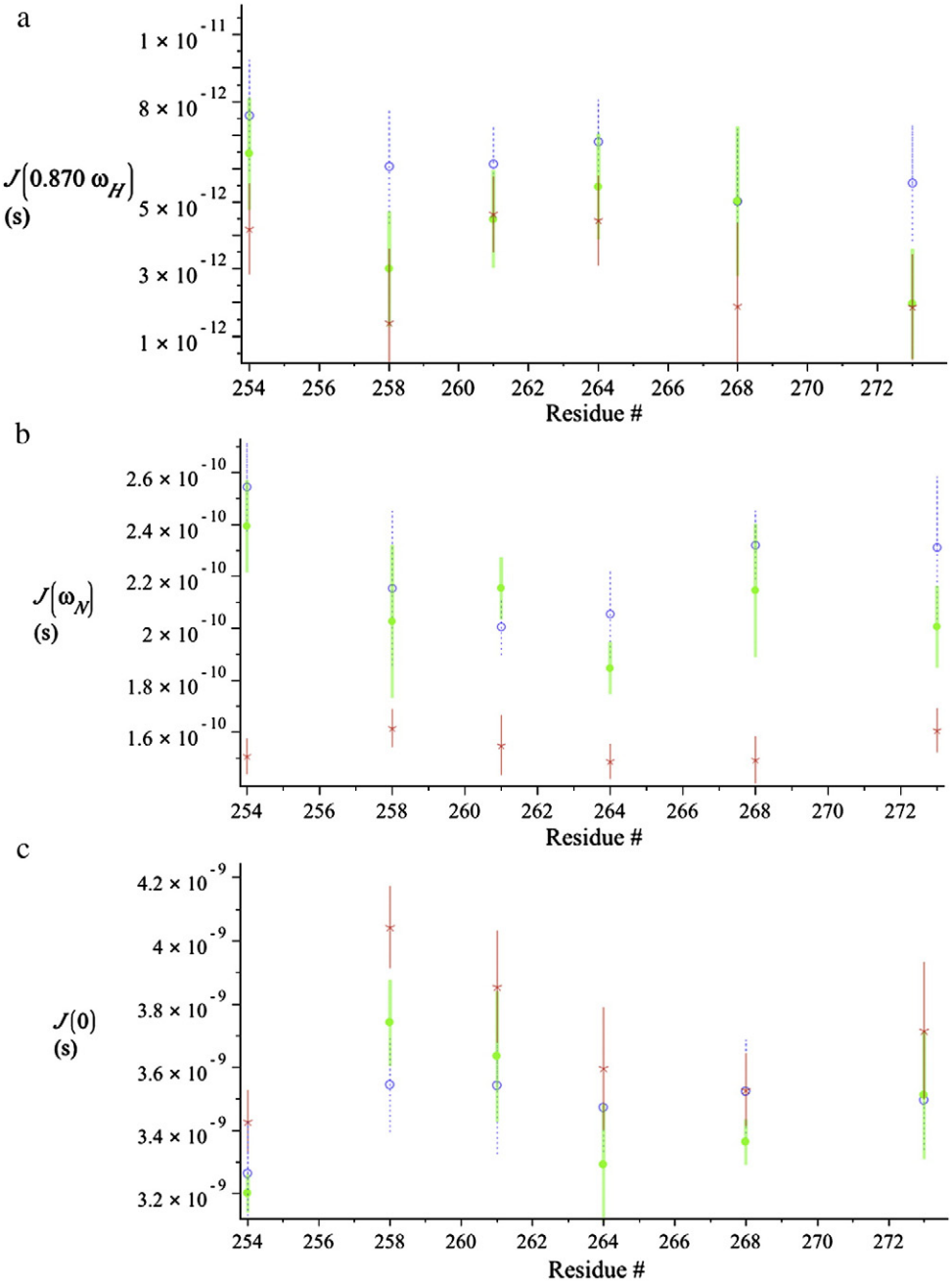

Fig. 3. Spectral density functions for the six ^{15}N-labelled residues of the TM VII peptide. (a) Plot of $J(0.87\omega_H)$ values, which represent the population of ^{15}N–H amide bond vectors rotating with a frequency of $0.870\omega_H$. $J(0.870\omega_H)$ was calculated by substituting measured T_1 and steady-state NOE values at three field strengths in to Eq. (8). (b) $J(\omega_N)$, which represents the population of ^{15}N–H amide bond vectors rotating in the intermediate frequency ω_N range. $J(\omega_N)$ was calculated by substituting measured T_1 and calculated $J(0.870\omega_H)$ values in to Eq. (9). (c) $J(0)$, which represents the contribution of restricted zero frequency 'motion' to the relaxation of ^{15}N. $J(0)$ was calculated by substituting experimental T_2 values and calculated $J(\omega_N)$ and $J(0.870\omega_H)$ values for each field strength in to Eq. (10). Symbols correspond to the proton Larmor frequency of the spectrometer used for the parameter measurements, with 500 MHz as (blue) open circles and dotted error bars, 600 MHz as (green) solid circles and wide/transparent error bars, and 800 MHz as (red) asterisks and solid error bars, respectively. The vertical error bars were produced by propagation of experimental uncertainty using Eq. (11).

chemical exchange since accurate quantification requires relaxation dispersion experiments [56,59].

3.4. Ile-scanning mutagenesis experiments

We examined five amino acids of TM VII and determined the effect of mutation of these amino acids to Ile. Initial experiments examined whether these mutant forms of the Na^+/H^+ exchanger expressed and targeted properly and had activity. Fig. 4a shows a representative Western blot of the expression of the stable cell lines containing the wild-type NHE1 and the mutant NHE1 expressed in AP-1 cells. Untransfected AP-1 cells showed no HA-tagged NHE1 protein. Wild-type NHE1 showed the characteristic two immunoreactive bands. One band represents fully glycosylated NHE1 and a second smaller immunoreactive band represents partial or deglycosylated NHE1 protein [15]. The mutants F260I, G261I, E262I and S263I all showed levels of NHE1 similar to that of controls, though varying with some expressing near equivalent amounts and others expressing higher or lower amounts of protein. The E262I mutant presented more deglycosylated NHE1 relative to the fully glycosylated protein and was expressed at a lower level than mutants F260I, G261I and S263I. A268I was unusual in that little NHE1 protein was expressed with an

Table 4
Per-residue model-free parameters and spectral density model selections.

Residue	Model	S^2	t_e (ps)	R_{ex} (s^{-1})
L254	2*	0.78 ± 0.01	40 ± 11	
L258	2*	0.89 ± 0.02	37 ± 229	
G261	4	0.65 ± 0.02	16 ± 5	1.9 ± 0.2
L264	4	0.75 ± 0.02	36 ± 8	0.6 ± 0.3
A268	4	0.76 ± 0.02	24 ± 13	0.5 ± 0.2
L273	1*	0.85 ± 0.02		

*These are the second most likely model choices based on the AIC selection within the Mathematica notebook which favored each residue in model five; however, the X^2 distributions were highly skewed for these fits, so the next most likely model was chosen. Also, model five has the most parameters (four) which can increase the strength of fit independent of its true reflection of the empirical relaxation data.

intermediate size. Eight independently made isolates showed this same expression pattern.

Mutation of transmembrane amino acids can affect surface targeting of the Na^+/H^+ exchanger [15] so we examined intracellular targeting of the various NHE1 expressing cell lines as described in Materials and methods. Cells were treated with sulfo-NHS-SS-biotin, and labelled proteins of lysates were collected by binding to streptavidin-agarose beads. Western blotting with anti-HA antibody examined levels of NHE1 in equal amounts of total cell lysates and unbound lysates. This allowed deduction of relative amounts of tagged intracellular NHE1 protein. Fig. 4b illustrates examples of the results and a summary of at least four experiments. Both the 110 kDa and 95 kDa bands were included in the analysis. The results indicate that, in all cases, mutation of the amino acids to Ile caused slight decreases in targeting of the protein to the plasma membrane. The A268I mutant was almost totally intracellular and showed no significant level at the cell surface. Non-specific binding of NHE1 protein to streptavidin-agarose beads was ~5%.

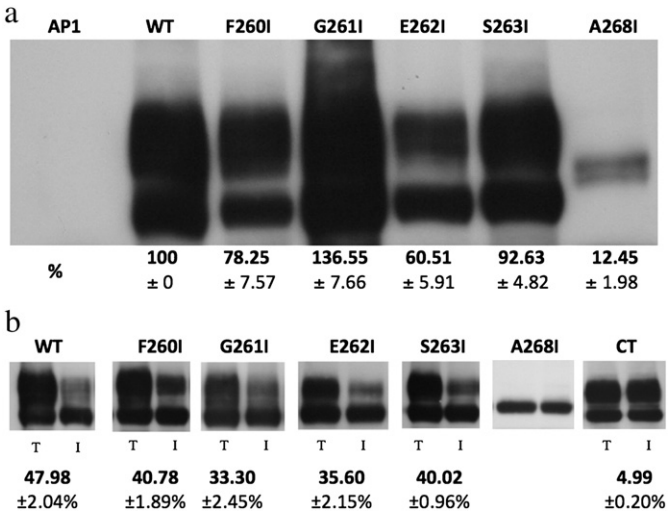

Fig. 4. Characterization of NHE1 expression in AP-1 cells. (a) Western blot analysis of cell extracts from control AP-1 cells and stably transfected AP-1 cells with Ile-scanning mutations in TM VII. Cell extracts were prepared from control and stably transfected cell lines and equal amounts of protein were separated by SDS-PAGE. Western blotting versus the HA tag identified NHE1 protein. Numbers below the lanes indicate the values obtained from densitometric scans of both the 110 kDa and 95 kDa bands relative to cysteineless NHE1. Results are mean ± the S.E. of at least 3 measurements. (b) Subcellular localization of control NHE1 and TM VII Ile-scanning mutants in AP-1 cells. Cells were treated with sulfo-NHS-SS-biotin and lysed. Then solubilized proteins were treated with streptavidin-agarose beads to bind labelled proteins and remove them from lysates. Equal samples of total cell lysate (left side of each panel) and unbound lysate (right side) were separated on SDS-PAGE. Western blotting was done with anti-HA antibody to identify NHE1. CT refers to an experiment in which non-specific binding to streptavidin-agarose beads was measured by following the standard procedure without labelling cells with biotin. WT, wild-type NHE1. Other mutants are as indicated. The percent of the total plasma membrane NHE1 protein that was found in each sample is indicated. The results are the mean ± the S.E. of at least 6 measurements.

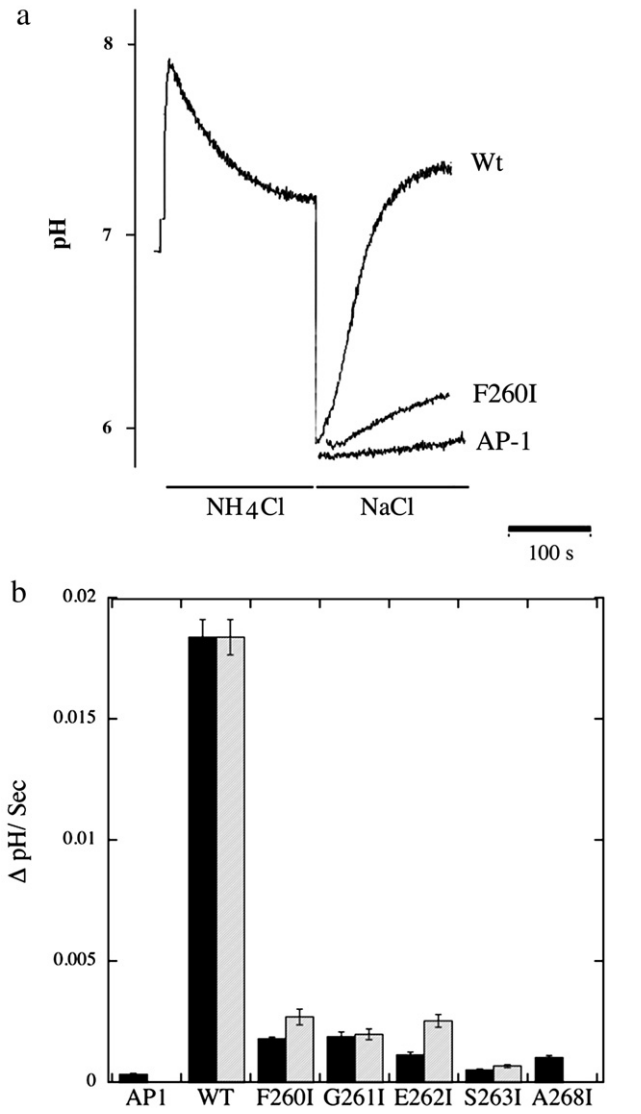

Fig. 5. Na^+/H^+ exchange activity measured for wild-type and Ile mutant NHE1 proteins stably transfected in AP-1 cells. (a) Na^+/H^+ exchanger activity was measured after ammonium chloride-induced acid load as described in Materials and methods, and a representative recovery curve is shown for NHE1 protein with the mutation F260I, relative to the cell line control (labelled AP1) and a wild-type (Wt) exchanger transfected into the AP-1 cell line. Periods of NH_4Cl, NaCl containing solution are indicated. For clarity only the recovery from acidosis is illustrated for F260I and AP-1 cells. (b) Summary of the rate of recovery from the acid load is shown for wild-type NHE1 protein, for all five Ile substitution mutants, and for the AP-1 cell line. Rates are either uncorrected (filled bars) or corrected (open bars) for protein expression and targeting relative to the wild-type AP-1 transfection. Results are mean ± SE of at least 8 determinations.

We next determined the effect of the mutations on NHE1 activity. NHE1 activity was measured as described earlier by examining the rate of recovery from an acute acid load induced by ammonium chloride [60]. Fig. 5 illustrates an example (Fig. 5a) and a summary (Fig. 5b) of the rates of recovery from stable cell lines transfected with wild-type Na^+/H^+ exchanger, or mutants of TM VII. We also show the rate of recovery corrected for both the level of expression and surface targeting. All of the mutants were severely affected by mutation to Ile. Correction for surface targeting and expression only slightly improved the relative activity of all these mutants. All five had less than 15% uncorrected activity compared to the wild-type NHE1 protein. Because their low activity made further experiments impractical, these mutants were not used for any further analysis. The A268I mutant was not corrected for

expression levels and targeting because targeting to the surface was not detectable in our assay.

4. Discussion

4.1. Relaxation parameters: comparing theory and experiment

The six ^{15}N-labelled residues of the TM VII peptide have similar values for all three relaxation parameters at each field strength (Fig. 2) suggesting similar flexibility on the ps–ns time scale along the length of the peptide (Fig. 1). Both T_1 and T_2 follow the expected theoretical trends within experimental error for relaxation time versus field strength at the experimentally determined rotational correlation time (τ_M) of ~10 ns. Analysis of the steady-state NOE is a bit more convoluted. The predicted trend is a decrease in the NOE with increasing field strength for a τ_e in the tens of ps range as estimated from model-free analysis (see Table 4) coupled with the experimentally estimated τ_M. However, experimentally we generally observe that NOE increases with field strength (Fig. 2c). It is possible that the effective internal correlation times are underestimated, in which case a τ_e of 350 ps would be sufficient to account for the experimentally observed trend. This is not surprising given the low precision in the τ_e estimations from model-free analysis (Table 4). Low τ_e precision from model-free analysis is especially pronounced for restricted residues ($S^2 \geq 0.8$) [54].

4.2. Reduced spectral density mapping

No significant differences were observed for $J(0.870\omega_H)$, $J(\omega_N)$ or $J(0)$ at a given field strength for the six ^{15}N-labelled residues (Fig. 3), again suggesting that motions on the ps–ns time scale are similar for the tested residues. The propagated errors at the three spectral density frequencies vary considerably, and also depend on the field strength of measurement. The former result is consistent with previous NMR dynamics analyses on a series of peptides where errors varied between negligible and large on a per-residue basis at a given spectral density frequency [61]. The most commonly used measure of structural flexibility in spectral density mapping is $J(0)$, the value of the function at zero frequency. It is normally interpreted as a measure of restricted motion, with large values suggesting increased local structure, and small values consistent with flexibility [56,61]. Chemical exchange (R_{ex}) and ^{15}N chemical shift anisotropy (CSA) variations along the primary sequence of the peptide may contribute to errors in $J(0)$ and may explain the deviations between field strengths we observed (Fig. 3c) for this theoretically field-independent parameter [56]. Specifically, $J(0)$ values calculated from higher field strength data are more susceptible to inflation by chemical exchange contributions to R_2 [56], and our $J(0)$ values are generally greater using 800 MHz data (Fig. 3c). $J(0)$ values are similar for all six ^{15}N-labelled residues (Fig. 3c), suggesting an equal degree of motional restriction on the ps–ns time scale. The slightly reduced order parameter for G261 does not contradict its $J(0)$ because chemical exchange can inflate the observed $J(0)$ [56,58]. If G261 is a pivot point allowing motion of the portions of TM VII C- and N-terminal to it relative to each other (Fig. 1), as we have previously suggested [12], the motion at this residue is most likely to be on the μs–ms time scale. This estimate of the motional time scale is based both on the observation of a single set of exchange-averaged chemical shifts despite extensive conformational sampling in the peptide apparent from nuclear Overhauser effect contacts [12] and on the mathematical fit of a chemical exchange term (R_{ex}) from model-free analysis (Table 4).

4.3. Functional analysis

When we examined the effect of replacement of five amino acids of TM VII with Ile we found that all of the mutants were impaired in function. We have previously examined TM VII and our results in this study complement these other studies well [12]. Mutation of the individual residues Phe260, Gly261 and Ser263 to Ala caused a decrease in activity of NHE1 [12], but not to as great an extent as the Ile mutations (for comparison see Table 5). This suggests that the bulkier Ile residue interferes more with NHE1 function [12,39]. In all cases, the effect of substitution to Ile was much greater than substitution to Ala. For example, substitution of F260 and G261 to Ala resulted in an NHE1 protein with approximately 30% of the activity of the wild type ([12]). Changing these amino acids to Ile left a protein with only approximately 10% of the wild-type activity. For S263, substitution to Ala left a protein with approximately 60% of the wild-type activity, but changing to Ile left a protein that was virtually inactive. In the case of E262, both Ala or Ile substitutions were nearly inactive, though in the case of Ala substitution much of this was due to changes in protein expression and surface targeting, while for Ile the changes were due to inactivity of the protein itself (Table 5).

The mutant A268I was unusual in its glycosylation, displaying an intermediate mobility and low expression levels (Fig. 4). This may be indicative of faulty processing, a conclusion that is supported by the fact that it was not targeted properly to the cell surface. The mutant E262I also displayed a somewhat unusual pattern in comparison with most of the other mutant proteins. It was expressed to a lower level than the other proteins but also showed a higher amount of higher mobility protein relative to the fully glycosylated protein. We previously [12,62] found that mutation of this residue to Cys caused the same phenomenon to occur to an even greater extent. In addition, with the change to Cys, surface targeting and expression levels were similarly impaired. We also found earlier [39] that mutation of this residue to Gln caused the same effects. Clearly this residue plays a key role in the function of the protein. In fact, in the most recent model of NHE1 activity, E262 is the principal residue involved in the initial coordination of a cytosolic proton [10] albeit under a different topology model than the widely accepted version of Wakabayashi et al. [11].

4.4. Correlating structure, dynamics, and function

The structure of TM VII in DPC micelles is an interrupted α-helix (Fig. 1). For a converged structural ensemble without discarding a significant portion (>34%) of the NOE contacts assigned, we had to employ a new dual-conformer calculation protocol [12,63]. Through parallel calculation of pairs of conformers, all NOEs were well satisfied, implying extensive conformational sampling about the G261–S263 region of the TM segment. The dual-conformer protocol is equally accommodating of pairs of non-interacting conformers existing simultaneously in the ensemble vs. oligomerization. Because NOEs were almost entirely satisfied through isolated dual conformers, rather than dimer formation, TM VII was attributed to be a monomer undergoing conformational exchange [12]. The TM VII peptide gave a

Table 5
Activity of NHE1 after Ile mutagenesis at NHE1 TM VII versus the previously reported Ala mutants [12].

Mutant mutation	Activity uncorrected		Activity corrected	
	Ala	Ile	Ala	Ile
F260	37.15 ± 3.2	9.88 ± .4	48.45 ± 1	14.79 ± .86
G261	26.48 ± 1.6	10.32 ± 1.1	39.46 ± 1	10.9 ± .31
E262	11.07 ± 2.4	6.25 ± .6	52.6 ± 1	13.9 ± 1.35
S263	58.5 ± 3.6	2.9 ± .25	89.97 ± 3	3.76 ± 3.3
A268	N/A	5.65 ± .45	N/A	–

Activity is given as a percent of wild-type NHE1 activity. Results are presented as mean ± SE of at least 8 determinations. Corrected and uncorrected refers to values obtained either with or without correcting for expression levels and surface targeting of the NHE1 protein.

single set of averaged chemical shifts, rather than multiple sets of independently sequentially assignable shifts implying distinct and long-lived conformations (*i.e.*, our recent structure of apelin-17 [64]). Chemical shift averaging demonstrates that interconversion between the two major conformers assumed by TM VII in micelles is rapid on the NMR time scale (~ms or faster).

Placing this in context of ^{15}N-backbone relaxation, the highly similar T_1, T_2, and steady-state NOE values imply highly similar dynamics at the ps–ns time scale along the length of the TM VII peptide. In light of both the chemical shift averaging and the lack of distinctive variations in ps–ns dynamics, conformational interconversion is therefore most likely to be in the μs–ms regime. To produce the observed dual-conformer set of TM VII structures, this exchange must be occurring in the G261–S263 region and is consistent with a chemical exchange model being selected from model-free analysis for residues G261, L264, and A268 (Table 4), with the largest R_{ex} parameter for G261. From these model-free results, a hypothetical mechanism is that the N-terminal region of TM VII is undergoing relatively little μs–ms level motion while the G261–S263 pivot point is allowing the C-terminal region containing L264 and A268 to exchange between two conformations (Fig. 1) relative to the N-terminus.

In order to consider the necessity of flexibility allowed by the break in helicity of the otherwise helical TM VII segment at residues G261–S263, we compare two sets of mutagenesis studies. E262 is not considered in this structural-dynamic correlation analysis, given the likelihood of involvement in ion translocation discussed above. There is perturbation to function with Ala mutation and almost complete loss of function with Ile mutation for the full-length NHE1 protein with mutation at F260, G261 and S263 (Table 5). Liu and Deber have tested the propensity for all 20 amino acids to form an α-helix in a hydrophobic environment [8,38]. Using these results, the effect of the various Ala and Ile mutations presented both previously [12] and herein can be examined in the context of a perturbation to the formation of a non-helical region. Mutation of F260, which is in the N-terminal α-helical region of TM VII, to Ala or Ile would be fairly non-perturbing in terms of secondary structure propensity and F260I reasonably conservative in terms of side-chain size; therefore, the loss of the F260 side-chain itself appears to be the critical feature of this mutation. Both G261A and G261I are relatively non-perturbing in terms of α-helical propensity in a membrane. For this position, therefore, the lack of steric constraint of a Gly residue seems likely to be the most important factor, correlating well to the break in helical structure and to the evidence for μs–ms scale dynamics at G261. S263 is sensitive to mutation to either Ala or Ile, with mutation to either residue significantly increasing helical propensity. A good possibility is that the Ala and Ile mutants are sufficiently perturbing to local structure to extend the helical segment beginning at L264 to include S263A or S263I. This would significantly perturb both structure and dynamics in the G261–S263 region.

We have now documented interruptions in the regular secondary structure of NHE1 TM segments IV, VII, IX, and XI [12–15]. It will be important to assess the theme of intermediate time scale motion about a pivot point such as that predicted herein with more detailed chemical exchange information by performing relaxation dispersion experiments [56,59]. Structural and dynamics characterization of mutant TM domains which are known to significantly perturb function are also a potentially valuable tool in terms of understanding these processes. Chemical exchange is entirely consistent with the alternating-access mechanism proposed for exposure of E262 to cytosolic protons during the ion translocation cycle of NHE1, where the residue is bent away from the cytosol in certain conformations [10]. An alternating-access mechanism was also proposed for the homologous NhaA protein on the basis of its crystal structure [4].

Acknowledgments

We thank Dr. Leo Spyracopolous for providing Mathematica notebooks and for useful discussion; Dr. Edward d'Auvergne for enlightening discussions; and, Jason Moses and Marc Genest for synthesis, purification, and characterization of peptides. We also thank the Canadian National High Field NMR Centre for use of their facilities which are supported by the Canadian Institutes of Health Research (CIHR) and the Alberta Heritage Foundation for Medical Research. TR is supported by a Natural Sciences and Engineering Research Council of Canada (NSERC) Canada Graduate Scholarship (CGS) M and is grateful for travel grants from Dalhousie University and the Nova Scotia Health Research Foundation (NSHRF). Research was supported by a Health Research Project from NSHRF to JKR; by funding from CIHR to LF; and, from CIHR and the Protein Engineering Network of Centres of Excellence to BDS.

References

[1] R.P. Riek, I. Rigoutsos, J. Novotny, R.M. Graham, Non-[alpha]-helical elements modulate polytopic membrane protein architecture, J. Mol. Biol. 306 (2001) 349–362.
[2] S. Yohannan, S. Faham, D. Yang, J.P. Whitelegge, J.U. Bowie, The evolution of transmembrane helix kinks and the structural diversity of G protein-coupled receptors, Proc. Natl. Acad. Sci. U. S. A. 101 (2004) 959–963.
[3] K. Palczewski, T. Kumasaka, T. Hori, C.A. Behnke, H. Motoshima, B.A. Fox, I.L. Trong, D.C. Teller, T. Okada, R.E. Stenkamp, M. Yamamoto, M. Miyano, Crystal structure of rhodopsin: a G protein-coupled receptor, Science 289 (2000) 739–745.
[4] C. Hunte, E. Screpanti, M. Venturi, A. Rimon, E. Padan, H. Michel, Structure of a Na+/H+ antiporter and insights into mechanism of action and regulation by pH, Nature 435 (2005) 1197–1202.
[5] M. Takahashi, Y. Kondou, C. Toyoshima, Interdomain communication in calcium pump as revealed in the crystal structures with transmembrane inhibitors, Proc. Natl. Acad. Sci. 104 (2007) 5800–5805.
[6] A. Yamashita, S.K. Singh, T. Kawate, Y. Jin, E. Gouaux, Crystal structure of a bacterial homologue of Na+/Cl-dependent neurotransmitter transporters, Nature 437 (2005) 215–223.
[7] T. Jin, L. Peng, T. Mirshahi, T. Rohacs, K.W. Chan, R. Sanchez, D.E. Logothetis, The [beta][gamma] subunits of G proteins gate a K+ channel by pivoted bending of a transmembrane segment, Mol. Cell 10 (2002) 469–481.
[8] L.P. Liu, C.M. Deber, Uncoupling hydrophobicity and helicity in transmembrane segments. Alpha-helical propensities of the amino acids in non-polar environments, J. Biol. Chem. 273 (1998) 23645–23648.
[9] R. Sadja, K. Smadja, N. Alagem, E. Reuveny, Coupling G[beta][gamma]-dependent activation to channel opening via pore elements in inwardly rectifying potassium channels, Neuron 29 (2001) 669–680.
[10] M. Landau, K. Herz, E. Padan, N. Ben-Tal, Model structure of the Na+/H+ exchanger 1 (NHE1): functional and clinical implications, J. Biol. Chem. 282 (2007) 37854–37863.
[11] S. Wakabayashi, T. Pang, X. Su, M. Shigekawa, A novel topology model of the human Na+/H+ exchanger isoform 1, J. Biol. Chem. 275 (2000) 7942–7949.
[12] J. Ding, J.K. Rainey, C. Xu, B.D. Sykes, L. Fliegel, Structural and functional characterization of transmembrane segment VII of the Na+/H+ exchanger isoform 1, J. Biol. Chem. 281 (2006) 29817–29829.
[13] B.L. Lee, X. Li, Y. Liu, B.D. Sykes, L. Fliegel, Structural and functional analysis of TM XI of the nhe1 isoform of the NA+/H+ exchanger, J. Biol. Chem. (2009) M809201200.
[14] T. Reddy, J. Ding, X. Li, B.D. Sykes, J.K. Rainey, L. Fliegel, Structural and functional characterization of transmembrane segment IX of the NHE1 isoform of the Na+/H+ exchanger, J. Biol. Chem. 283 (2008) 22018–22030.
[15] E.R. Slepkov, J.K. Rainey, X. Li, Y. Liu, F.J. Cheng, D.A. Lindhout, B.D. Sykes, L. Fliegel, Structural and functional characterization of transmembrane segment IV of the NHE1 isoform of the Na+/H+ exchanger, J. Biol. Chem. 280 (2005) 17863–17872.
[16] A.G. Palmer III, NMR probes of molecular dynamics: overview and comparison with other techniques, Annu. Rev. Biophys. Biomol. Struct. 30 (2001) 129–155.
[17] A.G. Palmer, J. Williams, A. McDermott, Nuclear magnetic resonance studies of biopolymer dynamics, J. Phys. Chem. 100 (1996) 13293–13310.
[18] D. Ma, T.S. Tillman, P. Tang, E. Meirovitch, R. Eckenhoff, A. Carnini, Y. Xu, NMR studies of a channel protein without membranes: structure and dynamics of water-solubilized KcsA, Proc. Natl. Acad. Sci. 105 (2008) 16537–16542.
[19] A.M. Slovic, H. Kono, J.D. Lear, J.G. Saven, W.F. DeGrado, Computational design of water-soluble analogues of the potassium channel KcsA, Proc. Natl. Acad. Sci. U. S. A. 101 (2004) 1828–1833.
[20] O.C. Andronesi, S. Becker, K. Seidel, H. Heise, H.S. Young, M. Baldus, Determination of membrane protein structure and dynamics by magic-angle-spinning solid-state NMR spectroscopy and #x2020, J. Am. Chem. Soc. 127 (2005) 12965–12974.
[21] H. Heise, W. Hoyer, S. Becker, O.C. Andronesi, D. Riedel, M. Baldus, Molecular-level secondary structure, polymorphism, and dynamics of full-length Œ ± -synuclein fibrils studied by solid-state NMR, Proc. Natl. Acad. Sci. U. S. A. 102 (2005) 15871–15876.

[22] U.H. Durr, L. Waskell, A. Ramamoorthy, The cytochromes P450 and b5 and their reductases-promising targets for structural studies by advanced solid-state NMR spectroscopy, Biochim. Biophys. Acta 1768 (2007) 3235–3259.
[23] J. Xu, U.H. Durr, S.C. Im, Z. Gan, L. Waskell, A. Ramamoorthy, Bicelle-enabled structural studies on a membrane-associated cytochrome B5 by solid-state MAS NMR spectroscopy, Angew. Chem., Int. Ed. Engl. 47 (2008) 7864–7867.
[24] A.S. Arseniev, I.L. Barsukov, V.F. Bystrov, A.L. Lomize, A. Ovchinnikov Yu, 1H-NMR study of gramicidin A transmembrane ion channel. Head-to-head right-handed, single-stranded helices, FEBS Lett. 186 (1985) 168–174.
[25] C.M. Franzin, P. Teriete, F.M. Marassi, Structural similarity of a membrane protein in micelles and membranes, J. Am. Chem. Soc. 129 (2007) 8078–8079.
[26] R.R. Ketchem, W. Hu, T.A. Cross, High-resolution conformation of gramicidin A in a lipid bilayer by solid-state NMR, Science 261 (1993) 1457–1460.
[27] S.J. Opella, F.M. Marassi, J.J. Gesell, A.P. Valente, Y. Kim, M. Oblatt-Montal, M. Montal, Structures of the M2 channel-lining segments from nicotinic acetylcholine and NMDA receptors by NMR spectroscopy, Nat. Struct. Biol. 6 (1999) 374–379.
[28] M. Katragadda, J.L. Alderfer, P.L. Yeagle, Assembly of a polytopic membrane protein structure from the solution structures of overlapping peptide fragments of bacteriorhodopsin, Biophys. J. 81 (2001) 1029–1036.
[29] M. Katragadda, A. Chopra, M. Bennett, J.L. Alderfer, P.L. Yeagle, A.D. Albert, Structures of the transmembrane helices of the G-protein coupled receptor, rhodopsin, J. Pept. Res. 58 (2001) 79–89.
[30] F.C.L. Almeida, S.J. Opella, fd coat protein structure in membrane environments: structural dynamics of the loop between the hydrophobic trans-membrane helix and the amphipathic in-plane helix, J. Mol. Biol. 270 (1997) 481–495.
[31] V.Y. Orekhov, K.V. Pervushin, D.M. Korzhnev, A.S. Arseniev, Backbone dynamics of (1–71)-and (1–36)bacterioopsin studied by two-dimensional 1H-15N NMR spectroscopy, J. Biomol. NMR 6 (1995) 113–122.
[32] V.Y. Orekhov, D.M. Korzhnev, T. Diercks, H. Kessler, A.S. Arseniev, 1H–15N NMR dynamic study of an isolated α-helical peptide (1–36)-bacteriorhodopsin reveals the equilibrium helix-coil transitions, J. Biomol. NMR 14 (1999) 345–356.
[33] J. Orlowski, S. Grinstein, Na+/H+ exchangers of mammalian cells, J. Biol. Chem. 272 (1997) 22373–22376.
[34] S. Grinstein, D. Rotin, M.J. Mason, Na+/H+ exchange and growth factor-induced cytosolic pH changes. Role in cellular proliferation, Biochim. Biophys. Acta (BBA)-Rev. Biomembr. 988 (1989) 73–97.
[35] L. Shrode, A. Cabado, G. Goss, S. Grinstein, in: L. Fliegel (Ed.), The Na+/H+ Exchanger, R.G. Landes Co., Austin, TX, 1996, pp. 101–122.
[36] L. Fliegel, Regulation of myocardial Na+/H+ exchanger activity, Basic Res. Cardiol. 96 (2001) 301–305.
[37] M. Karmazyn, Q. Liu, X.T. Gan, B.J. Brix, L. Fliegel, Aldosterone increases NHE-1 expression and induces NHE-1-dependent hypertrophy in neonatal rat ventricular myocytes, Hypertension 42 (2003) 1171–1176.
[38] D.T. Jones, W.R. Taylor, J.M. Thornton, A model recognition approach to the prediction of all-helical membrane protein structure and topology, Biochemistry 33 (1994) 3038–3049.
[39] R. Murtazina, B.J. Booth, B.L. Bullis, D.N. Singh, L. Fliegel, Functional analysis of polar amino-acid residues in membrane associated regions of the NHE1 isoform of the mammalian Na+/H+ exchanger, Eur. J. Biochem. 268 (2001) 4674–4685.
[40] Y.P. Zhang, R.N. Lewis, R.S. Hodges, R.N. McElhaney, Interaction of a peptide model of a hydrophobic transmembrane alpha-helical segment of a membrane protein with phosphatidylethanolamine bilayers: differential scanning calorimetric and Fourier transform infrared spectroscopic studies, Biophys. J. 68 (1995) 847–857.
[41] L. Kay, P. Keifer, T. Saarinen, Pure absorption gradient enhanced heteronuclear single quantum correlation spectroscopy with improved sensitivity, J. Am. Chem. Soc. 114 (1992) 10663–10665.
[42] J.R. Taylor, An Introduction To Error Analysis, 2nd ed., University Science Books, Sausalito, CA, 1997.
[43] E.J. d'Auvergne, P.R. Gooley, Optimisation of NMR dynamic models II. A new methodology for the dual optimisation of the model-free parameters and the Brownian rotational diffusion tensor, J. Biomol. NMR 40 (2008) 121–133.
[44] E.J. d'Auvergne, P.R. Gooley, Optimisation of NMR dynamic models I. Minimisation algorithms and their performance within the model-free and Brownian rotational diffusion spaces, J. Biomol. NMR 40 (2008) 107–119.
[45] N.A. Farrow, R. Muhandiram, A.U. Singer, S.M. Pascal, C.M. Kay, G. Gish, S.E. Shoelson, T. Pawson, J.D. Forman-Kay, L.E. Kay, Backbone dynamics of a free and phosphopeptide-complexed Src homology 2 domain studied by 15N NMR relaxation, Biochemistry 33 (1994) 5984–6003.
[46] A. Abragam, The Principles of Nuclear Magnetism, Clarendon Press, Oxford, 1961.
[47] N.A. Farrow, O. Zhang, A. Szabo, D.A. Torchia, L.E. Kay, Spectral density function mapping using 15N relaxation data exclusively, J. Biomol. NMR 6 (1995) 153–162.
[48] Y. Hiyama, C.H. Niu, J.V. Silverton, A. Bavoso, D.A. Torchia, Determination of 15N chemical shift tensor via 15N–2H dipolar coupling in Boc-glycylglycyl[15N glycine]benzyl ester, J. Am. Chem. Soc. 110 (1988) 2378–2383.
[49] G. Lipari, A. Szabo, Model-free approach to the interpretation of nuclear magnetic resonance relaxation in macromolecules. 1. Theory and range of validity, J. Am. Chem. Soc. 104 (1982) 4546–4559.
[50] G. Lipari, A. Szabo, Model-free approach to the interpretation of nuclear magnetic resonance relaxation in macromolecules. 2. Analysis of experimental results. J. Am. Chem. Soc. 104 (1982) 4559–4570.
[51] L. Spyracopoulos, A suite of Mathematica notebooks for the analysis of protein main chain 15N NMR relaxation data, J. Biomol. NMR 36 (2006) 215–224.
[52] A.M. Mandel, M. Akke, A.G. Palmer III, Backbone dynamics of *Escherichia coli* ribonuclease HI: correlations with structure and function in an active enzyme, J. Mol. Biol. 246 (1995) 144–163.
[53] E.J. d'Auvergne, P.R. Gooley, The use of model selection in the model-free analysis of protein dynamics, J. Biomol. NMR 25 (2003) 25–39.
[54] A.G. Palmer, M. Rance, P.E. Wright, Intramolecular motions of a zinc finger DNA-binding domain from Xfin characterized by proton-detected natural abundance carbon-13 heteronuclear NMR spectroscopy, J. Am. Chem. Soc. 113 (1991) 4371–4380.
[55] J.F. Lefevre, K.T. Dayie, J.W. Peng, G. Wagner, Internal mobility in the partially folded DNA binding and dimerization domains of GAL4: NMR analysis of the N–H spectral density functions, Biochemistry 35 (1996) 2674–2686.
[56] V. Ropars, S. Bouguet-Bonnet, D. Auguin, P. Barthe, D. Canet, C. Roumestand, Unraveling protein dynamics through fast spectral density mapping, J. Biomol. NMR 37 (2007) 159–177.
[57] E.R. Slepkov, S. Chow, M.J. Lemieux, L. Fliegel, Proline residues in transmembrane segment IV are critical for activity, expression and targeting of the Na+/H+ exchanger isoform 1, Biochem. J. 379 (2004) 31–38.
[58] J.W. Peng, G. Wagner, Frequency spectrum of NH bonds in eglin c from spectral density mapping at multiple fields, Biochemistry 34 (1995) 16733–16752.
[59] F.A. Mulder, A. Mittermaier, B. Hon, F.W. Dahlquist, L.E. Kay, Studying excited states of proteins by NMR spectroscopy, Nat. Struct. Biol. 8 (2001) 932–935.
[60] X. Li, J. Ding, Y. Liu, B.J. Brix, L. Fliegel, Functional analysis of acidic amino acids in the cytosolic tail of the Na+/H+ exchanger, Biochemistry 43 (2004) 16477–16486.
[61] C.M. Slupsky, L. Spyracopoulos, V.K. Booth, B.D. Sykes, M.P. Crump, Probing nascent structures in peptides using natural abundance 13C NMR relaxation and reduced spectral density mapping, Proteins 67 (2007) 18–30.
[62] J. Ding, R.W. Ng, L. Fliegel, Functional characterization of the transmembrane segment VII of the NHE1 isoform of the Na+/H+ exchanger, Can. J. Physiol. Pharm. 85 (2007) 319–325.
[63] J.K. Rainey, L. Fliegel, B.D. Sykes, Strategies for dealing with conformational sampling in structural calculations of flexible or kinked transmembrane peptides, Biochem. Cell Biol. 84 (2006) 918–929.
[64] D.N. Langelaan, E.M. Bebbington, T. Reddy, J.K. Rainey, Structural insight into G-protein coupled receptor binding by apelin, Biochemistry 48 (2009) 537–548.